Saudi Pharmaceutical Journal 32 (2024) 102106

HOSTED BY

Contents lists available at ScienceDirect

Saudi Pharmaceutical Journal

journal homepage: www.sciencedirect.com

Original article

α-Glucosidase, butyrylcholinesterase and acetylcholinesterase inhibitory activities of phenolic compounds from *Carthamus tinctorius* L. flowers: *In silico* and *in vitro* studies

Jawaher A.M. Alotaibi [a], Alaa Sirwi [a], Ali M. El-Halawany [b], Ahmed Esmat [c], Gamal A. Mohamed [a], Sabrin R.M. Ibrahim [d,e], Abdulrahim A. Alzain [f], Taher F. Halawa [g], Martin Safo [h], Hossam M. Abdallah [a,*]

[a] *Department of Natural Products and Alternative Medicine, Faculty of Pharmacy, King Abdulaziz University, Jeddah 21589, Saudi Arabia*
[b] *Department of Pharmacognosy, Faculty of Pharmacy, Cairo University, Giza 11562, Egypt*
[c] *Department of Clinical Pharmacology, Faculty of Medicine, King Abdulaziz University, Jeddah 21589, Saudi Arabia*
[d] *Preparatory Year Program, Department of Chemistry, Batterjee Medical College, Jeddah 21442, Saudi Arabia*
[e] *Department of Pharmacognosy, Faculty of Pharmacy, Assiut University, Assiut 71526, Egypt*
[f] *Department of Pharmaceutical Chemistry, Faculty of Pharmacy, University of Gezira, Wad Madani 21111, Sudan*
[g] *Department of Pediatrics, Aberdeen Hospital, Newglasgow, Nova Scotia Health Authorities, Nova Scotia, Canada*
[h] *Department of Medicinal Chemistry, Center for Drug Discovery, School of Pharmacy, Virginia Commonwealth University, 800 East Leigh Street, Richmond, VA 23298, USA*

ARTICLE INFO

Keywords:
Safflower
Flavonoids
Alzheimer
Diabetes
Industrial development
Antioxidant

ABSTRACT

Chemical investigation of *Carthamus tinctorius* L. flowers resulted in isolation of seven metabolites that were identified as; *p*-Hydroxybenzoic acid (**1**), *trans* hydroxy cinnamic acid (**2**), kaempferol-6-C-glucoside (**3**), astragalin (**4**), cartormin (**5**), kaempferol-3-*O*-rutinoside (**6**), and kaempferol–3-*O*-sophoroside (**7**). Virtual screening of the isolated compounds against human intestinal α-glucosidase, acetylcholinesterase, and butyrylcholinesterase was carried out. Additionally, the antioxidant activity of the bioactive compounds was assessed. Compounds **1** and **5** exhibited moderate binding affinities to acetylcholinesterase (binding energy −5.33 and −4.18 kcal/mol, respectively), compared to donepezil (-83.33kcal/mol). Compounds **1**–**7** demonstrated weak affinity to butyrylcholinesterase. Compounds **2** and **4** displayed moderate binding affinity to human intestinal α-glucosidase,compared to Acarbose (reference compound), meanwhile compound **2** exhibited lower affinity. Molecular dynamic studies revealed that compound **4** formed a stable complex with the binding site throughout a 100 ns simulation period. The *in-vitro* results were consistent with the virtual experimental results, as compounds **1** and **5** showed mild inhibitory effects on acetylcholinesterase (IC_{50}s 150.6 and 168.7 μM, respectively). Compound **4** exhibited moderate α-glucosidase inhibition with an IC_{50} of 93.71 μM. The bioactive compounds also demonstrated notable antioxidant activity in ABTS [2,2′-azino-bis(3-ethylbenzothiazoline-6-sulfonic acid)], ORAC (oxygen radical-absorbance capacity), and metal chelation assays, suggesting their potential in improving dementia in Alzheimer's disease (AD) and mitigating hyperglycemia.

1. Introduction

The advancement of neurological disorders and other illnesses is attributed to oxidative stress caused by free radicals (Shah et al., 2014). During regular metabolic processes in the body, free radicals are produced and typically eliminated by the immune system's antioxidant enzymes (e.g., catalase, superoxide dismutase, glutathione, and hydroperoxidase). However, if there is an overproduction of free radicals or a weakened immune system, the neutralization of free radicals becomes inadequate, resulting in oxidative stress. This imbalance has been extensively studied and has been found to play a significant role in the development and progression of Alzheimer's disease (AD). The occurrence of oxidative stress leads to elevated oxidation levels in brain lipids, carbohydrates, proteins, and DNA. As a consequence, certain

* Corresponding author.
E-mail address: hmafifi@kau.edu.sa (H.M. Abdallah).

https://doi.org/10.1016/j.jsps.2024.102106
Received 25 March 2024; Accepted 15 May 2024
Available online 16 May 2024

byproducts of oxidation have been identified in the primary histopathological changes observed in Alzheimer's disease (AD), such as neurofibrillary tangles (NFTs) and senile plaques (Huang et al., 2016). Additionally, amyloid beta (Aβ) buildup is a hallmark of Alzheimer's disease (AD), leading to the deterioration of neurons and the release of excessive free radicals, and eventually resulting in mitochondrial dysfunction and inflammation (Abdallah et al., 2021; Sirwi et al., 2021). Furthermore, AD is identified by a lack of acetylcholine (ACh) at the synaptic cleft. Therefore, the management of Alzheimer's disease (AD) includes the inhibition of oxidative stress, as well as targeting the enzymes responsible for the breakdown of acetylcholine (ACh), namely acetylcholinesterase (AChE) and butyrylcholinesterase (BChE) (Ahmad et al., 2020; Amin et al., 2020).

Moreover, elevated levels of ROS cause structural and functional modifications to cellular proteins and lipids, resulting in impaired cellular function. Consuming excessive high-fat and/or carbohydrate diets has been shown to promote oxidative stress, as evidenced by higher levels of lipid peroxidation products, and reduced antioxidant status. In the context of obesity, chronic oxidative stress and the resulting inflammation are key factors contributing to the development of various pathologies, including insulin resistance, disrupted metabolic pathways, and diabetes mellitus (DM) (Newsholme et al., 2016).

DM is a metabolic disorder that results in high levels of glucose in the body. It is a chronic condition caused by insufficient insulin production or the cells not responding to insulin properly. This leads to hyperglycemia after meals and can result in ketoacidosis and protein loss (Abdallah et al., 2011; Abdallah et al., 2016). A method for treating diabetes involves blocking the conversion of complex carbohydrates into simple sugars by inhibiting the enzymes α-glucosidase and α-amylase (Abdallah et al., 2022; Omar et al., 2022). Miglitol and acarbose, two commonly used α-glucosidase inhibitors, are associated with a range of side effects such as renal tumors, liver damage, abdominal discomfort, diarrhea, and gas. As a result, researchers are always on the lookout for better, safer options to help managing diabetes (Abdallah et al., 2022).

Natural products are highly regarded as a valuable resource for various molecules that exhibit favorable biological activities. Safflower, scientifically known as *Carthamus tinctorius* L., is an annual herb that belongs to the Asteraceae family (Ren et al., 2017). Safflower is a versatile crop that serves multiple economic purposes. The seed contains high percentage of fixed oil rich in unsaturated fatty acids, in addition to alkaloids. Flavonoids represent the major constituent of the flower in addition to phenylethanoid glycosides, coumarins, steroids, and polysaccharides (Zhang et al., 1997; Gecgel et al., 2007; Xuan et al., 2018; Farag et al., 2020; Hegazi et al., 2022). The primary flavonoid found in Safflower is a form of C-glycosides that contain a quinochalcone nucleus. These bioactive compounds, including hydroxysafflor yellow A and carthamin, are responsible for the cardioprotective properties of *C. tinctorius* (Yue et al., 2013). In addition, the flavonoid may also contain the common O-glycosides as shown in luteolin, kaempferol, naringenin, hyperoside, and quercetin (Zhang et al., 2016). Safflower flowers have long been utilized in traditional practices across various cultures as a dye in the clothing industry and as a colorant in food (Bacchetti et al., 2020). Flowers' yellow color is due to the presence of hydroxysafflor yellow A, safflomin C, anhydrosafflor yellow B, isosafflomin C, safflor yellow B, and safflor yellow A. The red pigment of the flower is known as carthamin (Adamska and Biernacka, 2021). These phenolics have garnered significant interest for their potential health benefits, including antioxidants, anti-inflammatory, and other bioactivities.

Safflower has been shown to reduce cardiovascular and cerebrovascular diseases and providing health benefits to the functions of heart and brain cells, due to its high flavonoid content. Moreover, it can provide protection to the lungs, liver, and bones, and has anti-inflammation, anti-oxidant and anti-cancer properties (Xian et al., 2022). *C. tinctorius* has also been suggested as a potential treatment for AD, operating through various mechanisms such as inhibiting Aβ aggregation, reducing hyperphosphorylation of tau protein, enhancing cholinergic neurotransmitter levels, mitigating oxidative stress, combating neuroinflammation, improving synaptic plasticity, and preventing apoptosis (Liang and Wang, 2022). Among the various constituents of *C. tinctorius*, only carthatins-1 and -2, kaempferol, and luteolin were assessed for their inhibitory activity against AChE (Liang and Wang, 2022). Furthermore, previous studies have demonstrated the inhibitory activity of *C. tinctorius* against α-glucosidase (Hong et al., 2021). This activity has been attributed to serotonin derivatives that were isolated from the seeds of the plant (Asgarpanah and Kazemivash, 2013).

Various scientific exploration on the chemical profile of the *C. tinctorius* flowers and their health benefits may lead to the discovery of new therapeutic agents and further validate their potential uses.

Computers have become a crucial component of the drug discovery process for several reasons. Access to three-dimensional structures and the utilization of computational techniques have greatly enhanced our comprehension of drug targets, resulting in more cost-effective drug development process. As a result, computer-aided-drug-design (CADD) has become an integral component of drug discovery projects in both research institutions and the pharmaceutical industry. This, in turn, facilitates the more efficient discovery of potential drugs tailored to these targets (Baig et al., 2018).

The documented inhibitory effects of *C. tinctorius* on both AChE and α-glucosidase prompted the authors to undertake this study. Moreover, investigating the antioxidant activity of isolated compounds can provide valuable insights into the mechanisms by which these bioactive compounds contribute to the management of Alzheimer's disease (AD) and diabetes. Therefore, this study aimed at separation and characterization of the primary phenolic components found in *C. tinctorius* flowers, then virtual screening of the isolated compounds against C-terminal-domain of human intestinal α-glucosidase, acetylcholinesterase and butyrylcholinesterase from the Protein Data Bank (PDB) for their modulatory effects. Following, the compounds with promising activity were tested *in vitro* for their corresponding enzymes activities as well as the antioxidant effects.

2. Material and methods

2.1. General experimental techniques

The Bruker-Avance DRX-850 MHz spectrometer (Bruker BioSpin-Billerica- MA- USA) was used for the NMR study. Precoated TLC Silica gel plates and Silica gel 60 were employed for TLC and column chromatographic analyses, respectively (Merck- Darmstadt- Germany). The compounds were detected by measuring UV absorbance at λ_{max} 255 and 366 nm and heating at 110 C for 1–2 min, after spraying with a p-anisaldehyde:H_2SO_4 spray reagent.

2.2. Extraction and isolation procedure

Carthamus tinctorius L. flowers were purchased from local market in Jeddah, Saudi Arabia. The sample was authenticated by Prof. Rim Hamdy (Prof. of plant taxonomy and flora, Department of Botany and Microbiology, Faculty of Science, Cairo University). A specimen (CTS-10-43) was maintained at the Department of Natural Products and Alternative Medicine, King Abdulaziz University, Saudi Arabia.

Dried plant material (250 g) was extracted with methanol (4 × 500 mL, 48 h each), and evaporated using a rotary evaporator apparatus under low pressure at 40 °C to give a dry brown methanol extract (52 g). Total extract was suspended with water and defatted with n-hexane (40 mg), to give aqueous mother liquor (10 g). The aqueous part was chromatographed on polyamide column, using water and methanol as solvents, to obtain five fractions (20 %, 40 %, 60 %, 80 %, and 100 %).

Fraction 2 (40 %, 2.1 g) was subjected to SiO_2 column

chromatography (300 g × 50 cm × 3 cm) employing $CHCl_3$-MeOH (9.5–0.5) gradients to get 54 subfractions. Similar Subfractions were pooled together based on TLC, and under UV light and *p*-anisaldehyde spray reagent to give compound **1** (20 mg, white powder) and compound **2** (13 mg, white amorphous powder).

Fraction 3 (60 %, 3.3 g) was subjected to SiO_2 CC (300 g × 50 cm × 3 cm) using $CHCl_3$: MeOH (8.5:1.5) gradients, 44 subfractions were obtained based on collecting 100 mL fractions and monitoring them using TLC plates and UV light. Subfractions 9–13 were collected based on TLC plates (15 mg, amorphous yellow solid) to give compound **3** (6 mg, yellowish white powder). Subfractions 19–25 were collected based on TLC plates to give compound **4** (20 mg, yellow crystal) and was further purified by subjecting to Sephadex column chromatography using methanol mobile phase. Subfractions 31–36 were gathered based on TLC plates to obtain compound **5** (25 mg, yellow solid).

Fraction 4 (80 %, 2.2 g) was subjected to SiO_2 CC (300 g × 50 cm × 3 cm) using MeOH: $CHCl_3$- (2:8) gradients to obtain 25 subfractions. Subfractions 10–17 were subjected to Sephadex column chromatography using methanol as mobile phase, to give compound **6** (30 mg, yellow powder). Subfractions 19–23 were subjected to Sephadex column chromatography using methanol solvent, to give compound **7** (25 mg, yellow powder).

2.3. Proteins and ligands preparation

The 3-D structures of the C-terminal-domain of human intestinal α-glucosidase (ID:3TOP), acetylcholinesterase (PDB Code: 4EY7), and butyrylcholinesterase (ID: 4BDS) were obtained from the PDB. To ensure the accuracy and reliability of these protein structures, we processed and prepared them utilizing the Protein Preparation Wizard (PPW) within the Schrodinger software.

In this process, we added hydrogen atoms to the carbon atoms and gradually minimized the structures with the OPLS4 force field, ensuring that the RMSD did not exceed 0.30 Å. The minimization step was crucial for resolving any steric conflicts between atoms. During the refinement, we excluded water and other molecules. Different tautomers were generated using the Epik module in Schrödinger.

The compounds were prepared using the LigPrep module in Maestro. This encompassed adding hydrogen atoms and producing low-energy conformers, followed by energy minimization utilizing the OPLS4 with standard parameters. Lastly, we generated receptor grids around the bound ligands for the subsequent studies.

2.4. Molecular docking and MM-GBSA calculations

The ligand and the references molecules were docked into the active site of the three proteins using the Extra Precision (XP) Glide docking.

The docked compounds were then submitted to the Prime MM-GBSA (Molecular Mechanics-Generalized Born Surface Area) calculations. The binding energy determined by the Prime MM-GBSA of Maestro provided a reliable prediction of the binding affinity.

The MM-GBSA method incorporates several components, including OPLS4 MM energies, a VSGB solvation model, and a nonpolar solvation expression (GNP) that considers nonpolar SASA and van der Waals interactions.

2.5. Molecular dynamics (MD) simulation

We further investigated the most favorable docking poses of compound **4** and the reference compound, which were identified initially in our docking experiments using molecular dynamics (MD) simulations with the Academic Desmond software.

In setting up the system, we followed the System Setup protocol, immersing the ligand–protein complex within an orthorhombic box that had a 10 Å buffer region separating protein atoms from the box boundaries, which was then filled with an appropriate number of water molecules. We adopted the TIP3P model and the OPLS4 force field for our MD computations, and assigned partial charges based on the OPLS4 force field. To maintain system neutrality, we introduced the necessary counter ions (Na+ and Cl−) to achieve a 0.15 M salt concentration. We used an isothermal-isobaric (NPT) ensemble, controlling the temperature at 300 K and the pressure at 1.01325 bar. Our simulation lasted for 100 ns, with trajectory data saved every 100 picoseconds. For short-range van der Waals and Coulomb interactions, we applied a cutoff radius of 9.0 Å. To accurately evaluate electrostatic interactions, we applied the Particle Mesh Ewald method. The system was then subjected to minimization and equilibration processes, following the default protocols of the Desmond software. For in-depth analysis of our simulation data, we utilized the Desmond package's Simulation Interaction Diagram protocol. This tool allowed us to gain valuable insights from our trajectory files.

2.6. Assessment of acetylcholinesterase and butyrylcholine esterase inhibitory effects

The ability of isolated compounds to inhibit the enzymatic activity of acetylcholinesterase in-vitro was investigated as reported previously (Ellman et al., 1961; Osman et al., 2014). In brief, the assay depends on addition of DTNB (5,5′-dithiobis-(2-nitrobenzoic acid) indicator solution (prepared as 0.4 mM in tris buffer (100 mM), pH 7.5) to acetylcholine esterase (from *Electrophorus electricus* Cat#3389, sigma aldrich) solution (prepared as 0.02 U/mL final concentration in 50 mM tris buffer, pH7.5 with 0.1 % w/v BSA) in a 96-well plate. Samples were prepared at final concentrations ranging from 500 to 31.25 µM. Donepezil was used as the standard anticholinesterase. Then, samples and donepezil were mixed with the indicator/enzyme solution for 15 min at room temperature. Subsequently, the substrate acetylcholine iodide (0.4 mM in tris buffer) was immediately added, and plate incubated in a dark for 20 min at room temperature. The developed color was then measured at 412 nm using multimode-microplate reader (Fluostar omega/BMG Labtech/Ortenberg Germany). The measured data were analyzed to calculate the inhibitory IC_{50} for each compound. The same procedure was applied for assessing the effect on butyrylcholine esterase activity but by using butyrylcholine esterase to prepare the enzyme solution and butyrylcholine iodide as a substrate.

2.7. Assessment of α-glucosidase inhibitory effect

The enzymatic activity of α-glucosidase was investigated in- as reported previously (Abdallah et al., 2022). Principally, the assay depends on adding p-NPG (p-nitrophenyl β-D-glucopyranoside) substrate solution (prepared as 3.0 in mM phosphate buffer (100 mM)/pH 7.0) to α-glucosidase solution (*Saccharomyces cerevisiae*, Sigma Aldrich, Cat# G5003) (prepared as 0.6 U/mL final concentration in 100 mM phosphate buffer, pH 7.0) premixed with standard/sample solutions, followed by 5-min incubation at 37 °C. Samples were tested initially at concentrations of 1000 µM to calculate percentage inhibition, then samples with potential inhibitory effect were tested at the range (25–1000 µM). Acarbose was used as the standard α-glucosidase inhibitor at the concentration range of 15.6–250 µM. The release of p-nitrophenol from the pNPG substrate was then recorded at 405 nm, utilizing multimode-microplate reader (Fluostar omega/BMG Labtech/Ortenberg/Germany). The measured data were analyzed to calculate the inhibitory IC_{50}.

2.8. Assessment of antioxidant capacity

The antioxidant capacities of isolated compounds were investigated by ABTS [2,2′-azino-bis(3-ethylbenzothiazoline-6-sulfonic acid)] and ORAC (oxygen radical-absorbance capacity) inhibitory tests. ABTS assay is based on the generation of a blue/green radical cation of 2,2′-azino-bis (3-ethylbenzothiazoline-6-sulfonic acid ($ABTS^{\cdot+}$) that can be reduced by

antioxidants (Arnao et al., 2001). The scavenging of $ABTS^{\bullet+}$ by tested compounds can be quantitatively detected at 734 nm. Trolox was used a standard antioxidant at a concentration range of 2.5–35 μM. The measured data were analyzed to calculate IC_{50} for each compound. On the other hand, ORAC test was done based on the method of Liang et al (Liang and Kitts, 2014). In brief, freshly prepared 2,2′-azobis (2-amidino-propane) dihydrochloride was utilized to generate peroxyl radicals that cause the decay of fluorescein substrate. The ability of tested compounds to delay the decay of fluorescein is directly correlated to their antioxidant capacity against the generated peroxyl radical. At emission (520 nm) and excitation (485 nm), fluorescence was measured. The findings were presented in terms of μM Trolox equivalent/mM sample. A multimode microplate reader was used for all measurements.

2.9. Assessment of metal chelating activity

Ferrozine Fe^{2+} chelation capacity was assessed *in-vitro* depending on the method of Santos et al. (Santos et al., 2017). Briefly, 0.05 mL samples/standard were pre-mixed with a 0.02 mL of $FeSO_4$ solution (0.3 mM in acetate buffer/pH 6). This allows Fe^{2+} ions chelation by the sample. The reaction was then initiated by the addition of 0.03 mL of ferrozine reagent (0.8 mM) and the mixture stirred and left standing for 10 min at room temperature. Samples were prepared at a concentration of 1 mg/mL in MeOH. EDTA was employed as the standard metal chelator at the concentration range (10–80 μM). Then, the decrease of color intensity was estimated at 562 nm to calculate the % inhibition for each sample, and the results expressed as μM EDTA equivalent/mg sample.

2.10. Statistical analysis

All IC_{50} data are represented as means ± SD, IC_{50} values and calculated using Graph pad Prism 8® by converting the concentrations to their logarithmic value and then selecting non-linear inhibitor regression equation (log inhibitor) vs normalized response-variable slope equation.

3. Results

3.1. Isolation of phenolic compounds from C. tinctorius

Chemical investigation of *C. tinctorius* flower led to isolation of *p*-Hydroxybenzoic acid (**1**) (Ibrahim et al., 2018), trans hydroxy cinnamic acid (**2**) (Miyake et al., 2012), kaempferol-6-C-glucoside (**3**) (Abdullah et al., 2016), kaempferol-3-O-glucoside (astragalin) (**4**) (Abdullah et al., 2016), cartormin (**5**) (Miyake et al., 2012), kaempferol-3-O-rutinoside (nicotiflorin) (**6**) (Dehaghani et al., 2017), and kaempferol–3-O-sophoroside (**7**) (Ibrahim et al., 2018) **(**Fig. 1 **).** Identity of the isolated compounds was confirmed by ^{1}H and ^{13}C NMR and compared with the reported values (Figs. S1–S20, Tables S1–S3).

3.2. Molecular docking and MM-GBSA calculations

The MM-GBSA (Molecular Mechanics-Generalized Born Surface Area) approach is a widely employed technique for the evaluation of the binding affinity between small molecules and proteins. In this study, we present MM-GBSA results based on the docking poses, as illustrated in Table 1**.** These results depict the free binding energies of compounds

Table 1
MM-GBSA free binding energies of compounds 1–7 and the references with the C-terminal domain of human intestinal α-glucosidase (PDB Code: 3TOP), acetylcholinesterase (PDB Code: 4EY7) and butyrylcholinesterase (PDB Code: 4BDS).

Compound	MMGBSA dG Bind (kcal/mol)		
	Acetylcholinesterase	Butyrylcholinesterase	α-glucosidase
1	−5.33	5.63	1.41
2	15.35	5.24	−4.46
3	24.76	30.75	49.17
4	33.32	29.01	−7.1
5	−4.18	22.17	39.04
6	24.19	25.06	13.85
7	34	56.08	23.44
Donepezil	−83.33	−13.71	–
Acarbose	–	–	−13.86

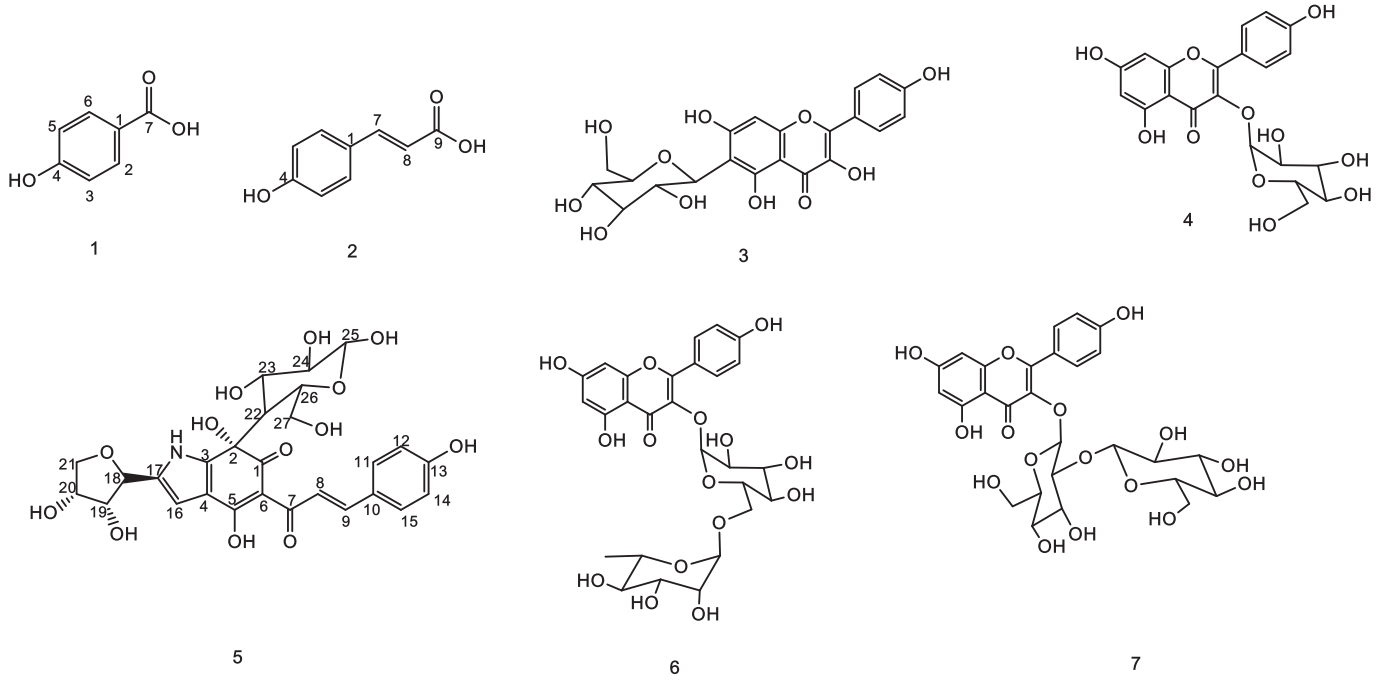

Fig. 1. Compounds (1–7) isolated from *C. tinctorius*.

1–**7**, in addition to the references Acarbose and Donepezil, when docked with C-terminal domain of human intestinal α-glucosidase, acetylcholinesterase, and butyrylcholinesterase. The binding energies are expressed in kilocalories per mole (kcal/mol), with more negative values indicating a stronger binding affinity to the target, while positive values signify less favorable binding interactions.

In our findings, all compounds **1**–**7** exhibit significantly lower binding affinities when compared to the reference compounds (Donepezil and Acarbose). Notably, Donepezil demonstrated a very strong favorable binding affinity to acetylcholinesterase, with a binding energy of −83.33 kcal/mol. Compounds **1** and **5** showed moderate binding affinities to acetylcholinesterase with a negative binding energy of −5.33 & −4.18 kcal/mol; respectively. On the other hand, compounds **1**–**7** displayed positive energy values when interacting with butyrylcholinesterase, suggesting unfavorable binding to the protein.

When examining their interactions with α-glucosidase, compound **4** displayed a moderate binding affinity with the protein with a binding energy of −7.1 kcal/mol. This compares with reference "Acarbose", which also showed very favorable binding affinity with a binding energy of −13.86 kcal/mol. As illustrated in Fig. 2, compound **4** is well-positioned within the binding cavity of α-glucosidase. It forms five hydrogen bonds with residues ASP1279, ASP1420, LYS1460, ARG1510, and ASP1526, in addition to engaging in two pi-pi interactions with TYR1251 (Fig. 3**)**. Furthermore, it interacts with numerous hydrophobic residues through hydrophobic contacts. In contrast, compound **2** displayed a relatively lower affinity with α-glucosidase, as indicated by a binding energy of −4.46 kcal/mol. The remaining compounds (**1**, **3**, **5**, **6**, and **7**) all exhibit positive binding energies, indicating unfavorable interactions with α-glucosidase.

3.3. Molecular dynamics (MD) simulations

Based on the binding affinity results, we chose compound **4** for further molecular dynamic studies to investigate its binding stability against α-glucosidase. Acarbose was studied as a reference. We selected the most promising docked conformation of compound **4**, and the co-crystal compound (Acarbose) for further 100 ns MD analysis.

We used three crucial measures to evaluate the stability of the protein-compound **4** complex. The first measure, RMSD, helps in assessing the stability of the protein in the presence of compound **4** over time. The data indicated only slight deviations. The RMSD values ranged from 1.2 Å to 2.4 Å, with a brief increase to 2.7 Å at 65 ns (as shown in Fig. 4). The reference compound exhibited similar fluctuations.

The second measure we used, RMSF, focuses on assessing how flexible the individual parts of the protein and compounds are within the complex. In our study, we found that the patterns of fluctuations in the protein with compound **4** and the reference were quite similar. The RMSF values ranged from 0.5 to 3.5 Å, as depicted in Fig. 5.

The third parameter we examined focuses on understanding the molecular interactions that occur during the simulation (Fig. 6**)**. Compound **4** formed significant interactions with ASP1157 (143 % H-bonds and 41 % water bridges), ASP1279 (92 % H-bonds and 43 % water bridges), and ASP1420 (100 % H-bonds). It also engaged in hydrogen bonds with LYS1460 (57 %). Furthermore, it established hydrophobic interactions with PHE1559 (85 %) and ARG1582 (39 %).

The reference compound exhibited interactions with ASP1279 via hydrogen bond interactions (100 %), with GLY1525 and primarily through water-bridge interactions (100 %), and with ASP1555 through water-bridge interactions (120 %). Additionally, the reference formed interactions with ARG1584 through predominantly hydrogen-bond interactions (100 %), and with HIS1584 through hydrogen-bond interactions (50 %).

3.4. Inhibition of acetylcholinesterase and butyrylcholinesterase

The effect of compounds that exhibited promising activity in computational study on acetylcholinesterase were assessed under similar experimental conditions. Donepezil was utilized as a reference anticholinesterase inhibitor with IC_{50} of 4.4 nM. Compounds **1** (*p*-Hydroxybenzoic acid) and **5** (cartormin) displayed mild inhibitory effects on acetylcholinesterase with IC_{50} values of 150.6 and 168.7 μM, respectively (Table 2). The rest of the compounds as expected from the virtual binding study did not show detectable inhibitory effect on butyrylcholinesterase, with IC_{50} values above 500 μM. Summarily, the experimental *in-vitro* studies correlated well with the virtual binding results.

3.5. Inhibition of α-glucosidase

As expected from the computational study, only compound **4**

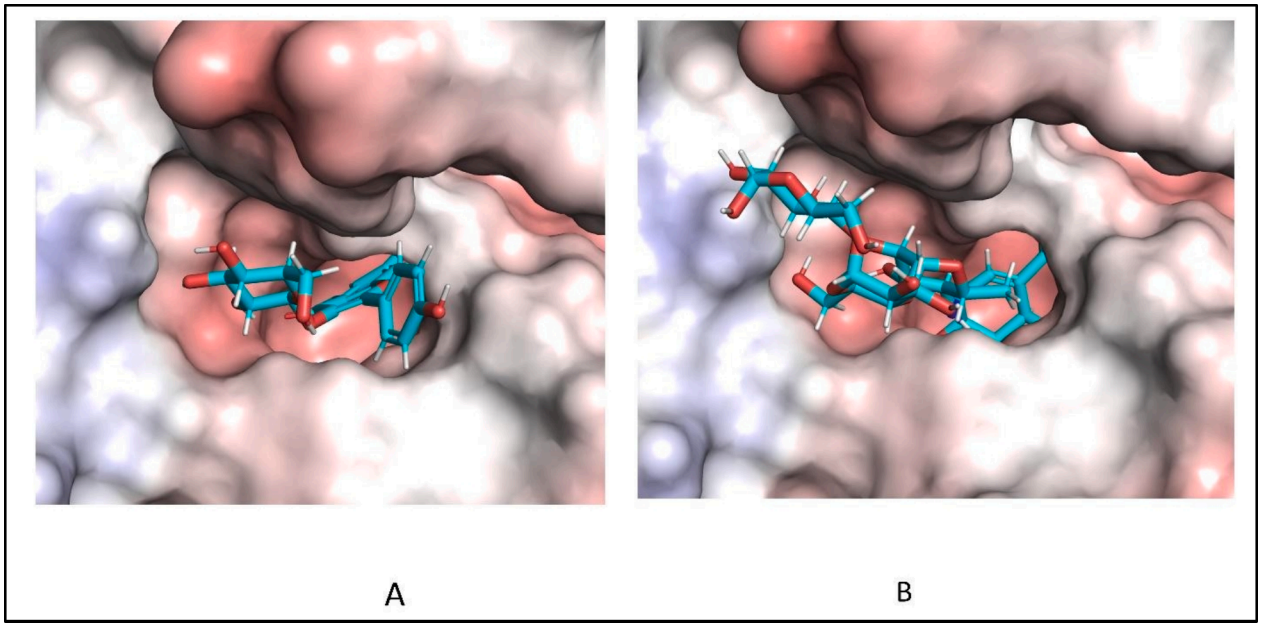

Fig. 2. 3D interactions of compound **4** (A) and the reference Acarbose (B) complexed with the human intestinal α-glucosidase (PDB Code: 3TOP).

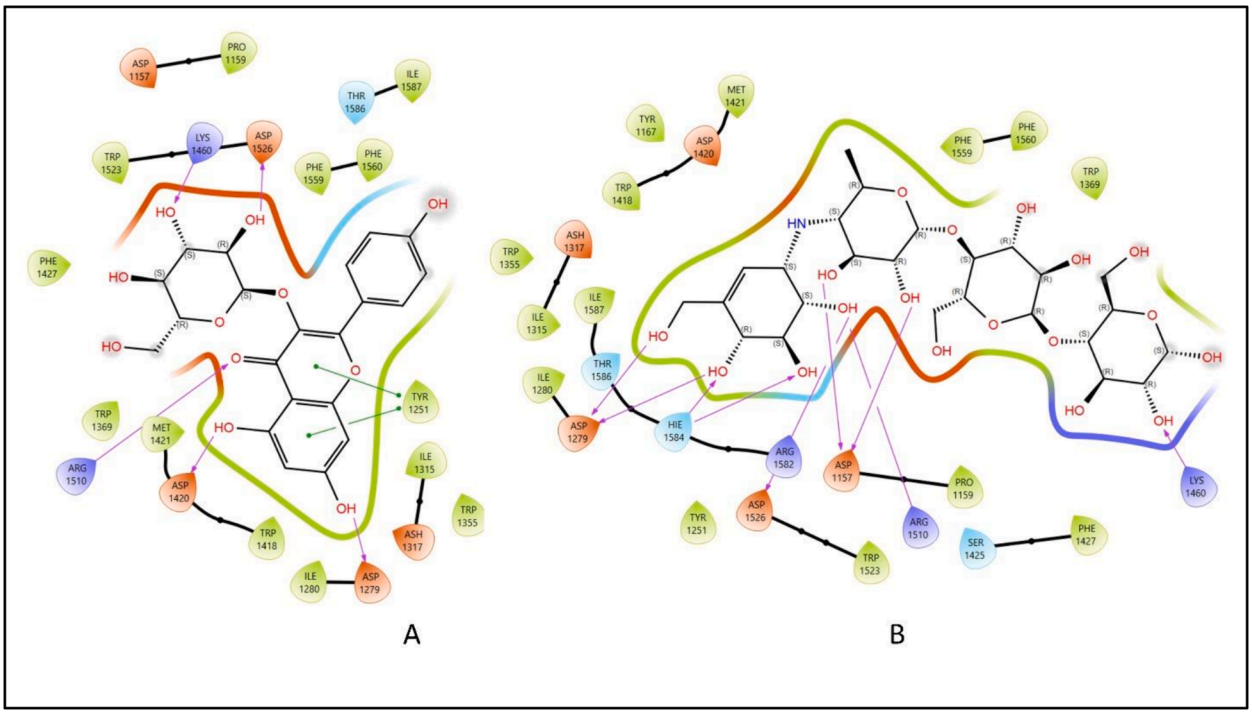

Fig. 3. 2D interactions of compound **4** (A) and the reference Acarbose (B) complexed with the human intestinal α-glucosidase (PDB Code: 3TOP).

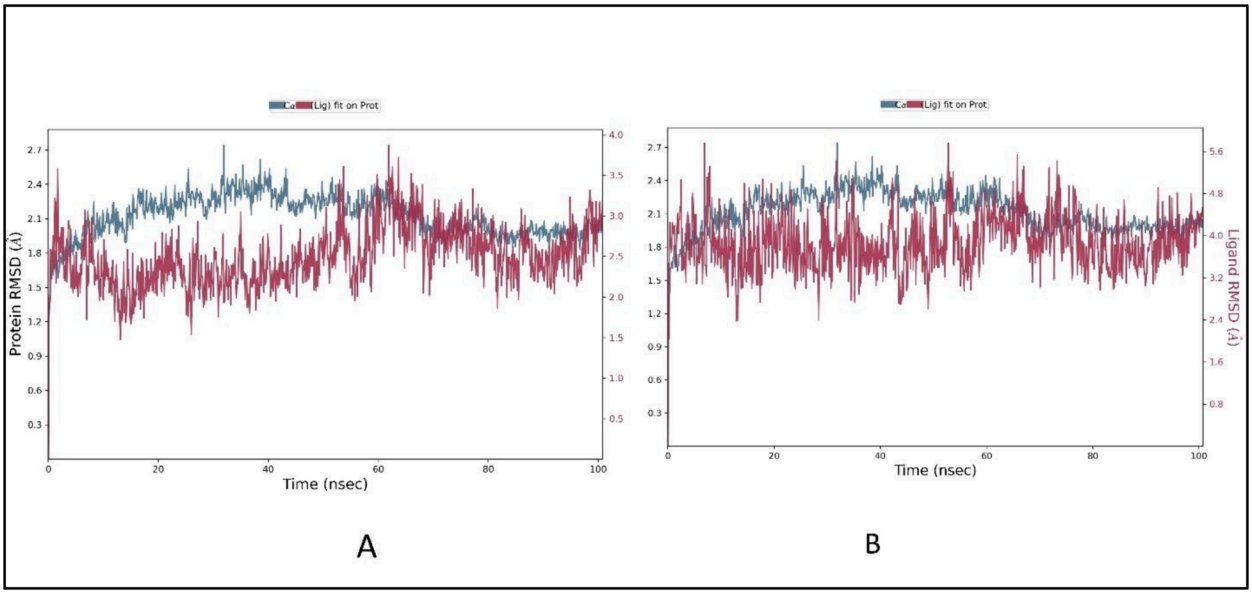

Fig. 4. The protein–ligand RMSD plot of compound **4** (A) and the reference Acarbose (B) complexed with the human intestinal α-glucosidase (PDB Code: 3TOP).

(Kaempferol-3-O-glucoside (astragalin)) demonstrated a potential inhibition of *α-glucosidase* with IC_{50} of 93.71 μM. The reference drug Acarbose inhibited α-glucosidase with IC_{50} of 66.63 μM.

3.6. Assessment of antioxidant and metal chelation activities

The antioxidant activities of isolated active compounds from *C. tinctorius* L. flowers were investigated by *in-vitro* assays, using ABTS, ORAC, and metal chelation techniques, as illustrated in Table 3**.** In the ABTS assay, compounds **5** was the most potent showing the least IC_{50} (17.84 μM) that is comparable to the reference Trolox (14.98 μM), followed by compounds **4** and **1** with IC_{50} 90.11 and 127 μM, respectively. In the ORAC assay, compound **4** "Kaempferol-3-O-glucoside" showed the highest activity (>10,000) in terms of μM Trolox equivalent per mM sample concentration, followed by compound **5** "cartormin" then compound **1** (*p*-Hydroxybenzoic acid) that showed about 50 % the activity of compound **4**. As for metal chelation, a similar pattern of activity was observed; where compound **4** "kaempferol-3-O-glucoside" possessed the highest iron-chelating effect, followed by **5** "cartormin", then compound **1** had about 27 % the activity of compound **4**.

4. Discussion

The aim of this study was to separate and identify the primary phenolic components found in *C. tinctorius* flowers, followed by virtual screening against C-terminal-domain of human intestinal α-glucosidase,

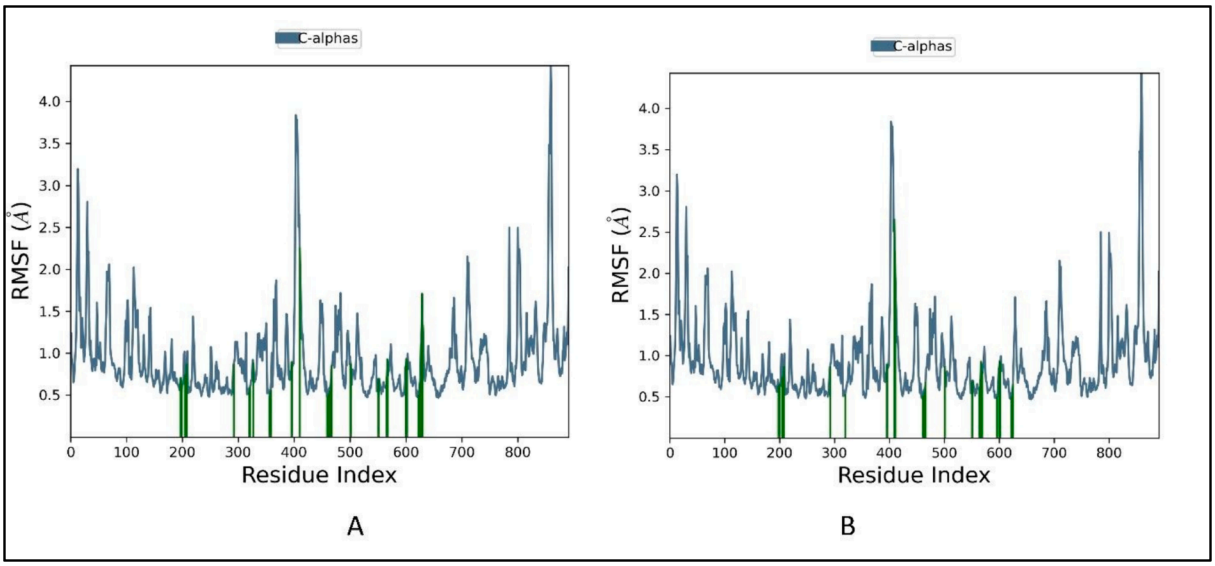

Fig. 5. Protein RMSF plot of the human intestinal α-glucosidase (PDB Code: 3TOP) in complex with compound **4** (A) and the reference Acarbose (B).

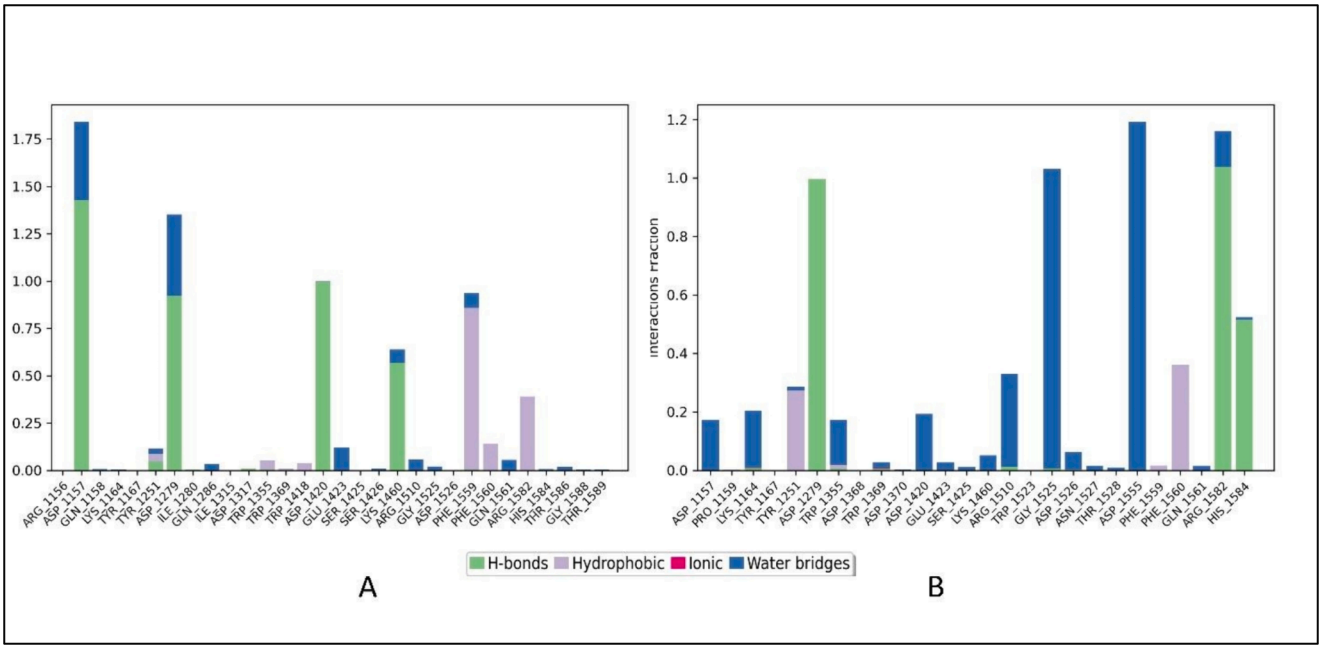

Fig. 6. Protein-ligand contact histogram of compound **4** (A) and the reference Acarbose (B) complexed with the human intestinal α-glucosidase (PDB Code: 3TOP) (Values over 100% are possible as some protein residue may make multiple contacts of same subtype with ligand).

Table 2
Effect of isolated compounds from *C. tinctorius* L. flowers on the enzymatic activities of acetylcholinesterase and butyrylcholinesterase.

Code	Compound	Acetylcholinesterase Inhibition Assay IC_{50} (μM)
1	p-Hydroxybenzoic acid	150.6 ± 10.3
5	Cartormin	168.7 ± 9.68
	Donepezil	0.0044 ± 0.0002

Data are presented as Mean ± S.D. n = 6.

acetylcholinesterase and butyrylcholinesterase crystal structures from the Protein Data Bank (PDB). Compounds with promising activity were further tested on the corresponding enzyme *in vitro* as well as assessing their antioxidant potential.

Inhibition of acetylcholinesterase is one of the approaches for symptomatic management of cognitive disorders like Alzheimer's disease. Based on the cholinergic hypothesis, dementia could be managed by elevating synaptic acetylcholine via inhibition of its specific enzyme acetylcholinesterase, leading to relative improvement of mental abilities (Cummings, 2021). There is a growing interest in medicinal plants with cholinergic properties due to their potential for fewer adverse effects compared to the conventional treatment options (Barut et al., 2017). The potential of *C. tinctorius* leaves and seeds to treat Alzheimer's disease (AD) has been demonstrated in earlier investigations through reducing amyloid β-level (Aβ) and inhibiting AChE activity, respectively (Liang and Wang, 2022). The seed extract also exhibited antioxidant effects by decreasing the production of ROS (reactive oxygen species) and raising antioxidant enzymes levels. Furthermore, the extract

Table 3
In-vitro assessment of antioxidant activities of isolated compounds from *Carthamus tinctorius* L. by: ABTS assay, ORAC assay, and metal chelation assay.

Code	Compound	ABTS assay IC_{50} (μM)	ORAC assay (μM Teq/mM)	Metal chelation (μM EDTA eq/mM)
1	p-Hydroxybenzoic acid	127.01 ± 10.98	5643 ± 333	12.20 ± 1.35
4	Kaempferol-3-O-glucoside	90.11 ± 2.97	10894 ± 442	44.48 ± 4.99
5	Cartormin	17.84 ± 0.23	9051 ± 152	37.45 ± 2.15
	Trolox	14.98 ± 0.603	—	—

The data is given as Mean ± S.D. for n = 6.

decreased β-and γ-secretases levels, leading to significant cognitive improvement in experimental animals. Additionally, certain key components isolated from *C. tinctorius* demonstrated anti-Alzheimer effects through multiple pathways, including inhibiting Aβ-aggregation, reducing hyperphosphorylation of tau protein, mitigating cholinesterase activity and oxidative stress, and exerting anti-inflammatory effects (Liang and Wang, 2022). Moreover, various dietary polyphenols (e.g., cinnamic aldehyde, rosmarinic acid, and ellagic acid) have been found to display neuroprotective and pro-cognitive activities in AD. These polyphenols act through several mechanisms, including modulating pro-oxidant/antioxidant machinery and inflammatory status (Caruso et al., 2022). It is noteworthy that the inhibitory activity of *C. tinctorius* against AChE was only evaluated for carthatins-1 and -2, kaempferol, and luteolin, which are among the different components found in *C. tinctorius*.

In this study, computational methods were employed for the evaluation of the binding mode and affinity between the isolated compounds and acetylcholinesterase and butyrylcholinesterase. In our findings, all compounds **1**–**7** showed significantly lower binding affinities when compared to Donepezil. Only compounds **1** and **5** exhibited moderate affinities for the enzyme acetylcholinesterase. Meanwhile, all isolated metabolites demonstrated positive energy values upon interaction with butyrylcholinesterase, suggesting unfavorable binding to this protein.

The *in-vitro* experimental findings aligned closely with the virtual binding outcomes. As anticipated based on the virtual binding study, the compounds exhibited no discernible inhibitory effect on butyrylcholinesterase, with IC_{50} values exceeding 500 μM. Meanwhile, compounds **1** and **5** exhibited moderate inhibitory effects on acetylcholinesterase, with IC_{50} values of 150.6 and 168.7 μM, respectively. To the best of our knowledge, this work is the first to describe the *in vitro* activity of cartormin (**5**) potential treatment of AD through the inhibition of acetylcholinesterase (AChE) activity. Meanwhile, *p*-Hydroxybenzoic acid (**1**) has been previously identified as an AChE inhibitor (Budryn et al., 2022) and here is the first report on its possible role in the activity of *C. tinctorius* in alleviating Alzheimer's disease (AD).

The antidiabetic effects of *C. tinctorius* flowers have been established, primarily attributed to its capacity to regenerate, and restore Langerhans islets, increasing insulin level. Moreover, it is also been shown to restore protein breakdown and enhancing glycogenesis in the livers of diabetic rats (Asgarpanah and Kazemivash, 2013). Recently, α-glucosidase inhibitory activity of its petal was reported (Hong et al., 2021). Computational studies revealed that compound **4** showed a highly favorable binding affinity with a binding energy of −7.1 kcal/mol against C-terminal domain of human intestinal α-glucosidase. Based on these findings, compound **4** was selected for further MD studies.

While the docking method offers valuable insights into binding poses, hydrogen bonds, and interactions with amino acid residues, it has certain limitations in capturing the flexibility of proteins. This limitation can impact on the accuracy of ligand–protein complexes and the stability and significance of these interactions over time. To address these issues, molecular dynamics (MD) simulation techniques were employed in this study. These simulations provided a more precise and comprehensive analysis by considering the dynamic nature of the system.

We selected the most promising docked conformation of compound **4**, and the co-crystal compound (Acarbose) for further 100 ns MD analysis. These selections were based on their favorable binding free energy, which makes them suitable candidates for in-depth examination. Compound **4** and Acarobose had RMSD values below 3 Å during the 100 ns of simulation, indicating a highly stable complex.

The RMSF values ranged from 0.5 to 3.5 Å. These values are well within the acceptable range for protein flexibility, indicating that the structures maintain the desired level of flexibility.

MD simulations offer us not only insights into the dynamic changes in the structure of molecules but also provide valuable information about the energy-related aspects of how a ligand interacts with a protein. This knowledge is of paramount importance when it comes to understanding the relationship between the structure and function of a target molecule and the specific nature of how a ligand binds to a protein. Therefore, we also used the MD simulation to provide an insight into the stability of interactions between compound **4**, Acarobose, and the protein during the simulation. The study showed that compound **4** and the protein interactions were primarily maintained through hydrogen bonds, water bridges, and hydrophobic interactions.

The *in vitro* assay results for compound **4** against α-glucosidase were consistent with the findings from the computational studies. Although α-glucosidase inhibitory activity of **4** was previously reported (Utari et al., 2019); our study provides molecular understanding of this inhibitory activity. Additionally, this study establishes a potential link between the inhibitory activity of α-glucosidase of *C. tinctorius* flowers and the presence of astragalin (**4**).

Indeed, α-glucosidase represents a principal enzyme for intestinal absorption of carbohydrates. This enzyme hydrolyzes oligosaccharides into individual glucose units to bind to glucose transporter prior to absorption. As an effective approach to control type-2 diabetes, α-glucosidase inhibition aims to reduce glucose level after meals (Sugihara et al., 2014).

It is worth noting that free radicals trigger the imbalance between prooxidant and antioxidant mechanisms intracellularly, leading to oxidative stress. Consequently, deterioration of cellular function becomes apparent and affects body organs, resulting in pathological conditions such as diabetes, Alzheimer's, Parkinson's, cardiovascular, rheumatoid arthritis, and cancer. This could further explain the potential ability of antioxidants to improve dementia in Alzheimer's disease and alleviate hyperglycemia in diabetes mellitus (Valko et al., 2007). In the current study, the formation of Fe^{2+}/ferrozine complex is diminished due to chelation of Fe^{+2} by antioxidants, expressed as μM EDTA equivalent per mM sample (Santos et al., 2017). The results of iron chelation are consistent with those of ORAC assay. The findings of this study are consistent with previous reports that have documented the antioxidant activity of phenolic acids (Manuja et al., 2013; Farhoosh et al., 2016), flavonoids (Amic et al., 2007), and C-glucosylchinochalcone (cartormin) (Vázquez et al., 2017).

5. Conclusion

In the present study, seven metabolites were isolated and identified from *C. tinctorius* flowers and were identified as: *p*-Hydroxybenzoic acid (**1**), *trans* hydroxy cinnamic acid (**2**), kaempferol-6-C-glucoside (**3**), astragalin (**4**), cartormin (**5**), kaempferol-3-*O*-rutinoside (**6**), and kaempferol–3-*O*-sophoroside (**7**). Virtually, compounds **1** and **5** exhibited moderate binding affinities to acetylcholinesterase compared to the reference compound donepezil while compound **4** showed a highly favorable binding affinity to human intestinal α-glucosidase. Furthermore, the *in vitro* evaluations of the active compounds

corroborated the findings from virtual studies with respect to enzymatic activities and antioxidant effects. These findings suggest the potential of these compounds in improving dementia associated with Alzheimer's disease (AD) and mitigating hyperglycemia in diabetes. These warrant further *in-vivo* studies to validate their anti-Alzheimer and anti-diabetes potential and to deeply understand their mechanisms of action.

Funding

The Deanship of Scientific Research (DSR) at King Abdulaziz University (KAU), Jeddah, Saudi Arabia has funded this project, under grant no. (RG-41-166-43). The authors, therefore, gratefully acknowledge DSR technical and financial support.

CRediT authorship contribution statement

Jawaher A.M. Alotaibi: Methodology, Formal analysis. **Alaa Sirwi:** Writing – review & editing, Supervision, Investigation. **Ali M. El-Halawany:** Methodology, Formal analysis. **Ahmed Esmat:** Writing – original draft, Formal analysis. **Gamal A. Mohamed:** Methodology, Formal analysis. **Sabrin R.M. Ibrahim:** . **Abdulrahim A. Alzain:** Methodology, Formal analysis. **Taher F. Halawa:** Validation, Investigation. **Martin Safo:** Methodology, Formal analysis. **Hossam M. Abdallah:** .

Data availability

Data will be made available on request.

Appendix A. Supplementary material

Supplementary data to this article can be found online at https://doi.org/10.1016/j.jsps.2024.102106.

References

Abdallah, H.M., Salama, M.M., Abd-Elrahman, E.H., et al., 2011. Antidiabetic activity of phenolic compounds from Pecan bark in streptozotocin-induced diabetic rats. Phytochem. Lett. 4, 337–341.
Abdallah, H.M., El-Bassossy, H., Mohamed, G.A., et al., 2016. Phenolics from *Garcinia mangostana* inhibit advanced glycation endproducts formation: effect on amadori products, cross-linked structures and protein thiols. Molecules 21, 251.
Abdallah, H.M., El Sayed, N.S., Sirwi, A., et al., 2021. Mangostanaxanthone IV ameliorates streptozotocin-induced neuro-inflammation, amyloid deposition, and tau hyperphosphorylation via modulating PI3K/Akt/GSK-3β pathway. Biology 10, 1298.
Abdallah, H.M., Kashegari, A.T., Shalabi, A.A., et al., 2022. Phenolics from *Chrozophora oblongifolia* aerial parts as inhibitors of α-glucosidases and advanced glycation end products: in-vitro assessment, molecular docking and dynamics studies. Biology 11, 762.
Abdullah, W., Elsayed, W.M., Abdelshafeek, K.A., et al., 2016. The flavonoids and biological activity of *Cleome africana* growing in Egypt. Res. J. Pharm., Biol. Chem. Sci. 7, 1092–1105.
Adamska, I., Biernacka, P., 2021. Bioactive substances in safflower flowers and their applicability in medicine and health-promoting foods. Int. J. Food Sci. 2021, 1–23.
Ahmad, S., Zeb, A., Ayaz, M., et al., 2020. Characterization of phenolic compounds using UPLC–HRMS and HPLC–DAD and anti-cholinesterase and anti-oxidant activities of *Trifolium repens* L. leaves. Eur. Food Res. Technol. 246, 485–496.
Amic, D., Davidovic-Amic, D., Beslo, D., et al., 2007. SAR and QSAR of the antioxidant activity of flavonoids. Curr. Med. Chem. 14, 827–845.
Amin, M.J., Miana, G.A., Rashid, U., et al., 2020. SAR based in-vitro anticholinesterase and molecular docking studies of nitrogenous progesterone derivatives. Steroids 158, 108599.
Arnao, M.B., Cano, A., Acosta, M., 2001. The hydrophilic and lipophilic contribution to total antioxidant activity. Food Chem. 73, 239–244.
Asgarpanah, J., Kazemivash, N., 2013. Phytochemistry, pharmacology and medicinal properties of *Carthamus tinctorius* L. Chin. J. Integr. Med. 19, 153–159.
Bacchetti, T., Morresi, C., Bellachioma, L., et al., 2020. Antioxidant and pro-oxidant properties of *Carthamus tinctorius*, hydroxy safflor yellow A, and safflor yellow A. Antioxidants 9, 119.
Baig, M.H., Ahmad, K., Rabbani, G., et al., 2018. Computer aided drug design and its application to the development of potential drugs for neurodegenerative disorders. Curr. Neuropharmacol. 16, 740–748.
Barut, E.N., Barut, B., Engin, S., et al., 2017. Antioxidant capacity, anti-acetylcholinesterase activity and inhibitory effect on lipid peroxidation in mice brain homogenate of *Achillea millefolium*. Turk. J. Biochem. 42, 493–502.
Budryn, G., Majak, I., Grzelczyk, J., et al., 2022. Hydroxybenzoic acids as acetylcholinesterase inhibitors: Calorimetric and docking simulation studies. Nutrients 14, 2476.
Caruso, G., Godos, J., Privitera, A., et al., 2022. Phenolic acids and prevention of cognitive decline: polyphenols with a neuroprotective role in cognitive disorders and Alzheimer's disease. Nutrients 14, 819.
Cummings, J., 2021. New approaches to symptomatic treatments for Alzheimer's disease. Mol. Neurodegener. 16, 1–13.
Dehaghani, Z.A., Asghari, G., Dinani, M.S., 2017. Isolation and identification of nicotiflorin and narcissin from the aerial parts of *Peucedanum aucheri* Boiss. J. Agric. Sci. Technol. 7, 45–51.
Ellman, G.L., Courtney, K.D., Andres Jr, V., et al., 1961. A new and rapid colorimetric determination of acetylcholinesterase activity. Biochem. Pharmacol. 7, 88–95.
Farag, M.A., Hegazi, N., Dokhalahy, E., et al., 2020. Chemometrics based GC-MS aroma profiling for revealing freshness, origin and roasting indices in saffron spice and its adulteration. Food Chem. 331, 127358.
Farhoosh, R., Johnny, S., Asnaashari, M., et al., 2016. Structure–antioxidant activity relationships of o-hydroxyl, o-methoxy, and alkyl ester derivatives of p-hydroxybenzoic acid. Food Chem. 194, 128–134.
Gecgel, U., Demirci, M., Esendal, E., et al., 2007. Fatty acid composition of the oil from developing seeds of different varieties of safflower (*Carthamus tinctorius* L.). J. Am. Oil Chem. Soc. 84, 47–54.
Hegazi, N.M., Khattab, A.R., Frolov, A., et al., 2022. Authentication of saffron spice accessions from its common substitutes via a multiplex approach of UV/VIS fingerprints and UPLC/MS using molecular networking and chemometrics. Food Chem. 367, 130739.
Hong, H., Lim, J.M., Kothari, D., et al., 2021. Antioxidant properties and diet-related α-glucosidase and lipase inhibitory activities of yogurt supplemented with safflower (*Carthamus tinctorius* L.) petal extract. Food Sci. Anim. Resour. 41, 122.
Huang, W.J., Zhang, X., Chen, W.W., 2016. Role of oxidative stress in Alzheimer's disease. Biomed. Rep. 4, 519–522.
Ibrahim, S.R., Abdallah, H.M., El-Halawany, A.M., et al., 2018. Thiotagetin B and tagetannins A and B, new acetylenic thiophene and digalloyl glucose derivatives from *Tagetes minuta* and evaluation of their in vitro antioxidative and anti-inflammatory activity. Fitoterapia 125, 78–88.
Liang, N., Kitts, D.D., 2014. Antioxidant property of coffee components: assessment of methods that define mechanisms of action. Molecules 19, 19180–19208.
Liang, Y., Wang, L., 2022. *Carthamus tinctorius* L.: a natural neuroprotective source for anti-Alzheimer's disease drugs. J. Ethnopharmacol., 115656
Manuja, R., Sachdeva, S., Jain, A., et al., 2013. A comprehensive review on biological activities of p-hydroxy benzoic acid and its derivatives. Int. J. Pharm. Sci. Rev. Res. 22, 109–115.
Miyake, Y., Ito, C., Itoigawa, M., 2012. A novel trans-4-hydroxycinnamic acid derivative from Meyer lemon (*Citrus meyeri*). Food Chem. 135, 2235–2237.
Newsholme, P., Cruzat, V.F., Keane, K.N., et al., 2016. Molecular mechanisms of ROS production and oxidative stress in diabetes. Biochem. J 473, 4527–4550.
Omar, A.M., AlKharboush, D.F., Mohammad, K.A., et al., 2022. Mangosteen metabolites as promising alpha-amylase inhibitor candidates: in silico and in vitro evaluations. Metabolites 12, 1229.
Osman, H., Kumar, R.S., Basiri, A., et al., 2014. Ionic liquid mediated synthesis of mono- and bis-spirooxindole-hexahydropyrrolidines as cholinesterase inhibitors and their molecular docking studies. Biorg. Med. Chem. 22, 1318–1328.
Ren, C.-X., Wu, Y.-Y., Tang, X.-H., et al., 2017. Safflower's origin and changes of producing areas. China J. Chin. Mater. Med. 42, 2219–2222.
Santos, J.S., Brizola, V.R.A., Granato, D., 2017. High-throughput assay comparison and standardization for metal chelating capacity screening: a proposal and application. Food Chem. 214, 515–522.
Shah, S.M.M., Sadiq, A., Shah, S.M.H., et al., 2014. Antioxidant, total phenolic contents and antinociceptive potential of *Teucrium stocksianum* methanolic extract in different animal models. BMC Complement. Altern. Med. 14, 1–7.
Sirwi, A., El Sayed, N.S., Abdallah, H.M., et al., 2021. Umuhengerin neuroprotective effects in streptozotocin-induced Alzheimer's disease mouse model via targeting Nrf2 and NF-Kβ Signaling cascades. Antioxidants 10, 2011.
Sugihara, H., Nagao, M., Harada, T., et al., 2014. Comparison of three α-glucosidase inhibitors for glycemic control and bodyweight reduction in Japanese patients with obese type 2 diabetes. J. Diabet. Invest. 5, 206–212.
Utari, F., Itam, A., Syafrizayanti, S., et al., 2019. Isolation of flavonol rhamnosides from *Pometia pinnata* leaves and investigation of α-glucosidase inhibitory activity of flavonol derivatives. J. Appl. Pharm. Sci. 9, 053–065.
Valko, M., Leibfritz, D., Moncol, J., et al., 2007. Free radicals and antioxidants in normal physiological functions and human disease. Int. J. Biochem. Cell Biol. 39, 44–84.
Vázquez, T.J.D., Cisneros, R.M.C., Guzmán, A.B.P., et al., 2017. Management of Orange (*Citrus sinensis*) wastes from agroindustrial activities using sustainable biodrying and composting processes. In: Agricultural Research Updates. Nova Science Publishers Inc, pp. 97–123.
Xian, B., Wang, R., Jiang, H., et al., 2022. Comprehensive review of two groups of flavonoids in *Carthamus tinctorius* L. Biomed. Pharmacother. 153, 113462.
Xuan, T.D., Gangqiang, G., Minh, T.N., et al., 2018. An overview of chemical profiles, antioxidant and antimicrobial activities of commercial vegetable edible oils marketed in Japan. Foods 7, 21.

Yue, S., Tang, Y., Li, S., et al., 2013. Chemical and biological properties of quinochalcone C-glycosides from the florets of *Carthamus tinctorius*. Molecules 18, 15220–15254.
Zhang, H.L., Nagatsu, A., Watanabe, T., et al., 1997. Antioxidative compounds isolated from safflower (*Carthamus tinctorius* L.) oil cake. Chem. Pharm. Bull. 45, 1910–1914.
Zhang, L.-L., Tian, K., Tang, Z.-H., et al., 2016. Phytochemistry and pharmacology of *Carthamus tinctorius* L. Am. J. Chin. Med. 44, 197–226.